Ab initio calculation of the electronic and optical properties of solid pentacene

Murilo L. Tiago,[1] John E. Northrup,[2] and Steven G. Louie[1]
[1]*Department of Physics, University of California at Berkeley, Berkeley, California 94720 and Materials Science Division, Lawrence Berkeley National Laboratory, Berkeley, California 94720*
[2]*Palo Alto Research Center, 3333 Coyote Hill Road, Palo Alto, California 94304*
(Received 08 November 2002; revised manuscript received 11 February 2003; published 31 March 2003)

The optical and electronic properties of crystalline pentacene are studied, using a first-principle Green's-function approach. The quasiparticle energies are calculated within the GW approximation and the electron-hole excitations are computed by solving the Bethe-Salpeter equation. We investigate the role of polymorphism on the electronic energy gap and linear optical spectrum by studying two different crystalline phases: the solution-phase structure and the vapor-phase structure. Charge-transfer excitons are found to dominate the optical spectrum. Excitons with sizable binding energies are predicted for both phases.

DOI: 10.1103/PhysRevB.67.115212 PACS number(s): 71.35.Cc, 78.20.Bh

I. INTRODUCTION

There has been an increase in interest in organic semiconductors for applications in electronic devices. Solid pentacene ($C_{22}H_{14}$) in particular has been the focus of much attention recently,[1–7] both as a model system for fundamental studies as well as a material employed in thin film growth of electronic devices.[8,9] An interesting and unsolved issue is the nature of charge transport in pentacene and other organic semiconductors. Both phonon-assisted hopping and band transport mechanisms have been discussed in the literature.[6,7,10] A deeper understanding of the transport mechanisms requires knowledge of the electronic excitations. We have therefore performed first-principle quasiparticle calculations of the band structure for pentacene employing the GW approximation. Two different crystalline phases have been studied: a bulk phase obtained by a solution-phase growth process[11] and a phase obtained by vapor deposition of molecular pentacene. The phase obtained by growth from solution, which we will denote *S*, was characterized structurally by Campbell, Robertson, and Trotter.[11] The phase obtained by vapor deposition, which we denote *V*, has been characterized by Siegrist *et al.*[1] Venuti *et al.*[5] have investigated the difference in the phonon spectrum for these two polymorphs, but there is limited knowledge of the effect of polymorphism on the electronic and optical properties of solid pentacene.

The calculations are performed by using first-principles methods. The structural properties are determined with the *ab initio* pseudopotential density functional method.[12] Quasiparticle energies are obtained by using the GW approach,[13] which provides a good description of electronic properties. We also calculate the linear optical response by solving the Bethe-Salpeter equation (BSE) for electron-hole excitations.[14] The effect of polymorphism is addressed by characterizing and comparing the electronic and optical properties of pentacene in structures *S* (solution-phase crystallized) and *V* (vapor-phase crystallized). This paper is organized as follows: Sec. II has a brief exposition of the theoretical approach employed. Electronic properties are presented in Sec. III, and the optical spectrum and exciton properties are discussed in Sec. IV. We conclude with some final remarks.

II. THEORY

The ground-state configuration of the system is described within the framework of density functional theory (DFT). Degrees of freedom related to core electrons can be ignored by replacing the electron-ion potential by *ab initio* pseudopotentials.[12] In the present work, we employ the generalized gradient approximation (GGA)[15] for the exchange-correlation potential V_{xc}, although similar results can be obtained using the simpler local-density approximation (LDA). The Troullier-Martins scheme[16] is used to generate the pseudopotentials, and we solve the Kohn-Sham equations, using a plane wave basis with energy cutoff of 50 Ry.

In order to obtain quasiparticle energies of electrons and holes, and thus determine the electronic band structure, we make use of the GW approximation for the electron self-energy operator Σ.[13] Within this approach, Σ is taken to be the first term in a series expansion in terms of the screened Coulomb interaction. Dielectric screening is calculated from first principles within the random phase approximation (RPA) and the generalized plasmon pole model for dynamical screening.[13] This formalism does not include electron-phonon interactions, which would lead to polarons, rather than electrons and holes, as the main single-particle excitations.

Optical excitations are obtained by including electron-hole correlations and solving the BSE for the two-particle Green's function.[14] The optical excitations may be written as a linear combination of electron-hole pairs plus corrections,

$$|S\rangle = \sum_{cv\mathbf{k}} A^S_{cv\mathbf{k}} \hat{a}^\dagger_{c\mathbf{k}} \hat{a}_{v\mathbf{k}} |G\rangle + \text{corrections}, \tag{1}$$

where $\hat{a}^\dagger_{c\mathbf{k}}$ creates an electron at empty band c with momentum $\mathbf{k}$ and $\hat{a}_{v\mathbf{k}}$ creates a hole at filled band v with momentum $\mathbf{k}$. $|G\rangle$ is the many-body ground state of the electronic system. The coefficients $A^S_{cv\mathbf{k}}$ satisfy the Bethe-Salpeter equation,

$$(\varepsilon_{c\mathbf{k}}-\varepsilon_{v\mathbf{k}})A^S_{cv\mathbf{k}}+\sum_{c'v'\mathbf{k}'}\mathcal{K}^{cv\mathbf{k}}_{c'v'\mathbf{k}'}A^S_{c'v'\mathbf{k}'}=E^S A^S_{cv\mathbf{k}}, \quad (2)$$

where E^S is the excitation energy of state $|S\rangle$, and $\mathcal{K}$ is the interaction kernel between electron and hole.[14] The first term in Eq. (2) refers to differences between quasiparticle energies. Once the electron-hole pair states ($A^S_{cv\mathbf{k}}$) and the excitation energies (E^S) have been determined, response functions can be calculated and compared with the experiment. The imaginary part of the dielectric function, $\epsilon_2(\omega)$, is given by

$$\epsilon_2(\omega)=\frac{4\pi^2e^2}{\omega^2}\frac{1}{V_c}\sum_S\left|\sum_{cv\mathbf{k}}A^S_{cv\mathbf{k}}\langle v\mathbf{k}|\boldsymbol{\lambda}\cdot\mathbf{v}|c\mathbf{k}\rangle\right|^2\delta(E_S-\omega), \quad (3)$$

where the velocity operator $\mathbf{v}$ is used instead of momentum because of the nonlocal nature of the quasiparticle theory (pseudopotentials and self-energy have nonlocal contributions).[17] λ is the polarization direction, and the crystal (or supercell) volume V_c normalizes the sum over excited states. From Eq. (3) and the Kramers-Kronig relations, one can obtain the real part of the dielectric function and other linear optical properties.

III. ELECTRONIC PROPERTIES

Polymorphism in pentacene is a known phenomenon, and a number of different crystalline structures has been observed and studied.[1–4,11] In the present work, we concentrate on two structures: structure *S*, obtained by crystallization of pentacene from solutions of trichlorobenzene;[11] and structure *V*, obtained by a vapor-phase deposition process.[1] Both structures have the same ''herringbone''-type arrangement of molecules, with two nonequivalent molecules per unit cell, space group *P*-1, and a triclinic crystalline lattice, but they have slightly different densities: 1.345 g/cm^3 and 1.361 g/cm^3 for structures *S* and *V*, respectively.[1,11] This difference in density gives rise to enhanced intermolecular interactions in structure *V* compared to *S*. As in other molecular solids, the pentacene molecules are bound together by weak Van der Waals interactions, and the cohesive energy itself is very small.[18]

A picture of the arrangement of molecules in the triclinic crystal is presented in Fig. 1. The unit cell is defined by the experimental parameters: $a=6.06$ Å, $b=7.90$ Å, $c=14.88$ Å, $\alpha=96.74°$, $\beta=100.54°$, $\gamma=94.2°$ for structure *S*, and $a=6.253$ Å, $b=7.786$ Å, $c=14.511$ Å, $\alpha=76.65°$, $\beta=87.50°$, $\gamma=84.6°$ for structure *V*.[1] In order to make comparisons easier, we use the lattice vector definition proposed by Siegrist *et al.*,[1] that differs from earlier ones[11] by the interchange of vectors *a* and *b*, and redefinition of vector *c*. In our calculations, we perform relaxation of atomic coordinates, keeping the cell parameters fixed at the experimental values. Within GGA, the calculated cohesive energies for the two structures are very similar.

Figure 2 presents the quasiparticle band structure for both systems, obtained from the GW calculation. Near the energy gap, electronic bands are arranged in pairs, and become almost degenerate at points *X*, *Y*, *A*, and *D*. The appearance of pairs of bands arises from the existence of two nonequivalent molecules in a unit cell. Intermolecular interactions break the two-fold degeneracy of the bands, and introduce finite bandwidths. As expected, structure *V* shows bigger bandwidths and a narrower energy gap. An analysis of electronic orbitals shows that the eight lowest empty bands and eight highest occupied bands are composed almost exclusively of combinations of carbon π orbitals. Energy bands far away from the energy gap have non-negligible σ character. Bandwidths are rather small along crystallographic direction *c* (Γ to *B* in Fig. 2), but they increase by one order of magnitude when going along directions *a* or *b*. For instance, the energy separation of bands for the highest occupied pair at point *E* is 0.54 eV for structure *V*. This strong anisotropy is consistent with what is known about the strength of intermolecular interactions along the various crystallographic planes.[18] Bandwidths of about 0.2 eV along direction *a* were also predicted by semiempirical Hartree-Fock calculations.[19]

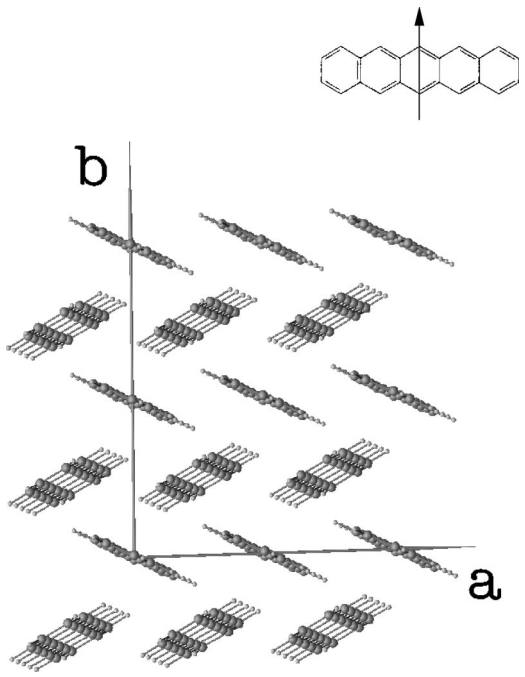

FIG. 1. Crystalline structure of solid pentacene projected on the *ab* plane. The molecules are arranged so that the long axis (along benzene rings) is roughly orthogonal to the *ab* plane. The short axis is indicated on the upper panel by an arrow.

Energy gaps obtained within GGA and the GW approximation are presented in Table I, together with bandwidths. Early photoconductivity measurements indicate an energy gap of 2.2 eV.[20] Within a specific band, the GW corrections are found to be roughly *k*-independent, and they can be approximated by a ''scissors operator.'' For structure *S* (*V* in parentheses), it has the form $\varepsilon^{GW}_{j\mathbf{k}}=\varepsilon^{DFT}_{j\mathbf{k}}+\varepsilon^{DFT}_{j\mathbf{k}}\times 0.22(0.23)$ for occupied bands, and $\varepsilon^{GW}_{j\mathbf{k}}=\varepsilon^{DFT}_{j\mathbf{k}}+1.30(1.13)+\varepsilon^{DFT}_{j\mathbf{k}}\times 0.10(0.17)$ for unoccupied bands, where all energies are given in *eV*. This procedure reproduces the GW quasiparticle energies to within 0.1 eV or less for energy bands within 5 eV from the gap. Outside this

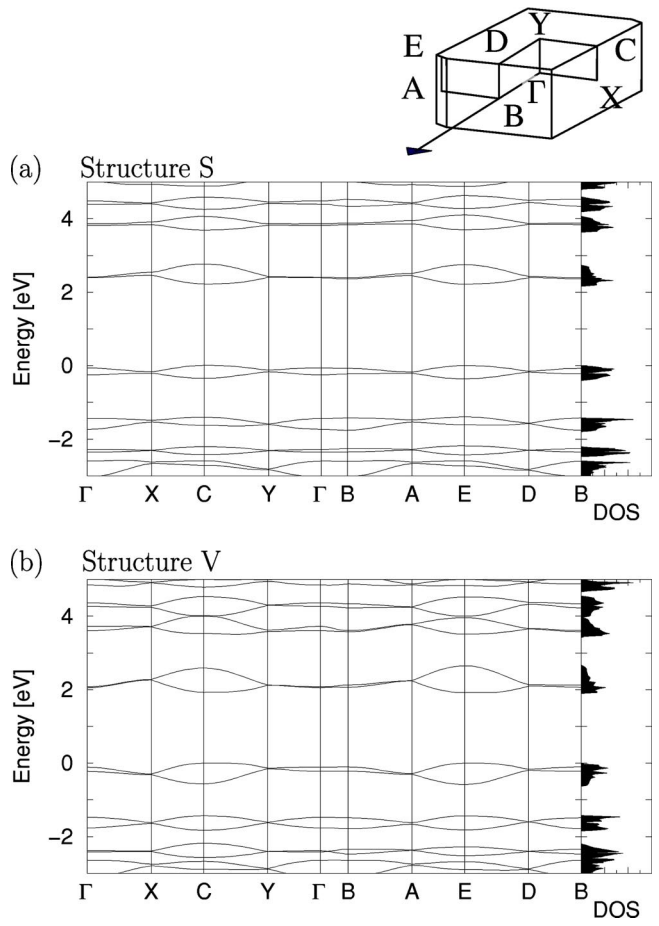

FIG. 2. Band structure of pentacene in structures *S* (a) and *V* (b). Only the bands close to the energy gap are shown. Energies are referenced to the valence band maximum. The density of states is shown in the right panel. The Brillouin zone (sketched in the inset) is oriented so that directions $\Gamma - X$ and $\Gamma - B$ are orthogonal to planes bc and ab, respectivelly.

range, the scissors approximation becomes more complicated due to the increasing σ character of energy bands. In the subsequent construction of the BSE, we make use of this scissors operator for states near the gap to facilitate the calculations.

TABLE I. Calculated GW energy gap and bandwidths *W* for the highest occupied pair of bands (HOMO) and the lowest unoccupied pair of bands (LUMO). *W* is defined to be the energy separation of the pairs of bands at the *E* point. For comparison, the Kohn-Sham gaps within the GGA are given in parenthesis. All quantities are in eV.

	Structure *S*	Structure *V*
W (HOMO)	0.36	0.54
W (LUMO)	0.57	0.67
energy gap	2.2	1.9
	(0.8)	(0.7)

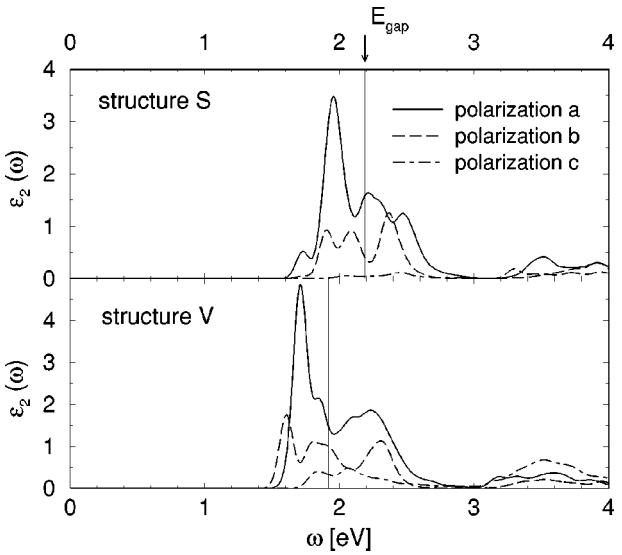

FIG. 3. Calculated imaginary part of the dielectric function for structures *S* (upper panel) and *V* (lower panel), for all three independent polarization directions. In each case, the quasiparticle energy gap is indicated by a vertical line.

IV. OPTICAL EXCITATIONS

We find the two structures studied to show similar optical spectra. The imaginary part of the calculated dielectric function is presented in Fig. 3 for polarization of light parallel to the three main crystallographic directions. For both the structures, several peaks below the quasiparticle energy gap appear and they correspond to optical transitions involving charge transfer excitons. In the energy range 1–4 eV, the weak absorption of light with polarization along direction *c* is a signature of the underlying molecular character of electronic states. For an isolated pentacene molecule, the highest occupied molecular orbital (HOMO) and lowest unoccupied molecular orbital (LUMO) states belong to group representations B_{1g} and B_{2u}, respectively (molecular pentacene itself belongs to symmetry group D_{2h}), and selection rules prevent optical transitions between these states with polarization perpendicular to the molecular short axis (see Fig. 1). The lower symmetry of the crystalline environment breaks this selection rule, resulting in weak optical activity for polarization along *c* and strong optical activity for polarization along *a*.

In the solution of the BSE, we use a discrete sampling of the Brillouin zone, with 384 regularly spaced *k*-points. This corresponds to a supercell of dimensions $8\times8\times6$, enough for a good description of charge transfer states with correlation length of about four molecules or less. The accuracy in the calculated quasiparticle excitation energies is about 0.1 eV, typical of the GW approximation, but exciton binding energies are accurate to within 0.02–0.04 eV. A comparison between density of excited states [obtained from Eq. (2) with the full interaction kernel $\mathcal{K}$], and the interband joint density of quasiparticle states (null kernel) shows that the absorption peaks below the gap in Fig. 3 are really due to discrete exciton states, instead of a continuum (see Fig. 4). As Eq. (3) shows, the density of excited states and the absorption spectrum differ by the oscillator strength contribution, related to

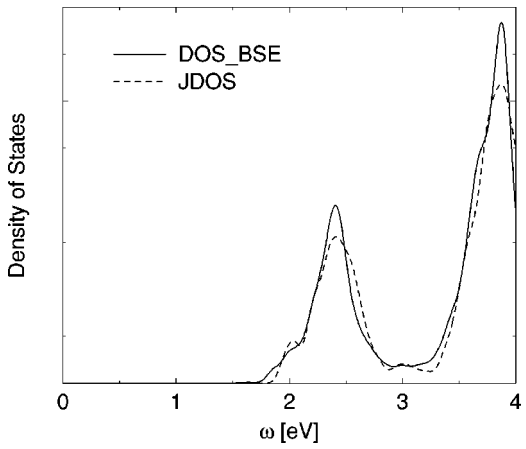

FIG. 4. Density of excited states obtained from the Bethe-Salpeter equation (solid line) and joint density of states (dashed line) for structure *V*. Both the functions are calculated with a Gaussian smoothing of 0.05 eV.

the coefficients $A^S_{cv\mathbf{k}}$. In Fig. 3, we include a Gaussian broadening of 0.05 eV in the (numerically discrete) absorption peaks. The measured width of the two lowest energy peaks is related to factors such as electron-phonon interactions and inhomogeneous broadening. Since these effects are ignored in the present work, the agreement between measured and calculated peak widths depends on our choice of the broadening parameter.

From the absorption spectrum, one can compute the refractive index and extinction coefficient. They are plotted in Fig. 5 for structure *V*. For the sake of comparison, we also include results obtained by ignoring electron-hole interactions [null kernel in Eq. (2)]. These quantities were measured in thin films of highly crystalline pentacene by Park *et al.*[22] Considering the difficulties both in experimental measurement and first-principles calculation of the dielectric function, one can see that the results from the present approach compare well with experiment, although the first exciton peak is found at 1.7 eV, whereas the measured data indicates 1.8 eV (see Table II). The broad features at 2.0–2.4 eV arise from the above gap transitions, and are consistent with what was seen in the experiment.

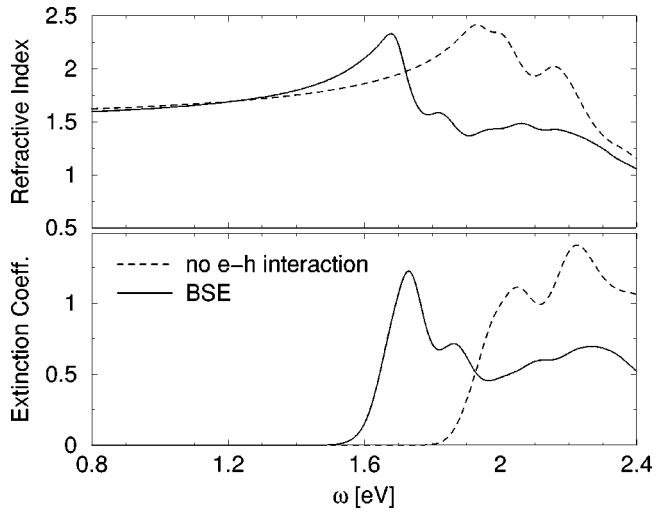

FIG. 5. Refractive index (upper panel) and extinction coefficient (lower panel) for structure *V*, polarization along direction *a*. Solid and dashed lines correspond to the results obtained from the Bethe-Salpeter equation and uncorrelated interband transitions, respectively.

TABLE II. Calculated energy position of the main features in the extinction coefficient (structure *V*), compared with the measurement by Park *et al.* (Ref. 22). All energies are in eV.

	Energy [eV]			
This work	1.73	1.86	2.13	2.27
Exp.[23]	1.82	1.94	2.11	2.25

The absorption spectrum obtained from structure *S* shows larger shifts compared with the measurements by Park *et al.*,[22] which suggests that structure *V* is similar to the crystalline phase present in the measured samples. Siegrist *et al.*[1] observed absorption in the range 1.8–2.5 eV and above 3.5 eV, which is also consistent with our calculations (see Figs. 3 and 5), although their measurement provides limited details.

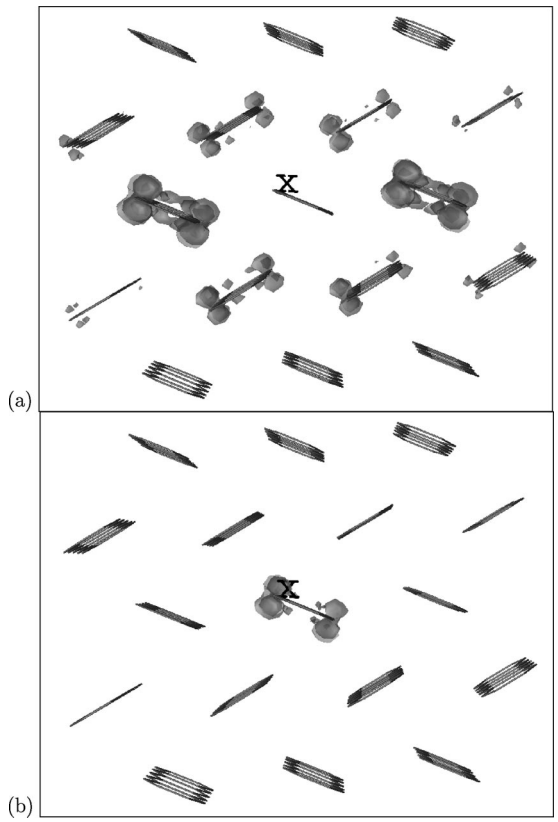

FIG. 6. Isovalue contour of the electron-hole probability distribution for the lowest spin singlet (a) and triplet (b) excitons. The value of the distribution at each contour is such that 30% of the integrated distribution is contained inside the contour. The crystalline structure is *V*, and the hole is fixed slightly above the molecule marked with an ''x.'' In both cases, the probability distribution is very small outside the shown molecular layer. Around a given molecule, this probability distribution resembles the distribution of the LUMO.

TABLE III. Calculated excitation energy of lowest spin singlet and triplet excitons, and Davydov splitting for the spin triplet states (energies are in eV).

	Structure *S*	Structure *V*
Singlet excitation energy	1.7	1.6
Triplet excitation energy	0.9	0.8
Davydov splitting (spin triplet)	0.05	0.08

Aoki-Matsumoto *et al.*[23] have also observed a well pronounced exciton line at 1.84 eV.

Spin triplet excitations may also be obtained within the BSE approach, differing from spin singlet excitations by the absence of a repulsive exchange interaction in the kernel K.[14] This state has binding energy of about 1 eV, with respect to the free electron and hole energies. Figure 6 illustrates the calculated electron-hole probability distribution for the lowest spin singlet and triplet states. Whereas the former one is a charge transfer exciton, the latter is a very well-localized Frenkel exciton. This difference in character is related to the exchange interaction, which effectively adds a repulsive potential between electron and hole.[14]

Table III shows the excitation energy of the lowest triplet exciton state, and the corresponding Davydov splitting.[6,21] The Davydov splitting[24] is small compared to typical bandwidths of pentacene because it is dominated by dispersion along direction $E-C$. Figure 2 does not show that dispersion explicitly, but the energy states at points E and C are less than 0.1 eV apart, whereas other crystallographic directions show dispersions much bigger than that. Early predictions of the Davydov splitting are around 0.1 eV.[21] Spin singlet states have much smaller binding energies, of about 0.3 eV measured from the electronic gap (Tables I and III). Table III shows that the excitation energy of the lowest spin singlet state is roughly twice the lowest spin triplet state. Recent pump-probe spectroscopy experiments on pentacene thin films have suggested this ratio of excitation energies, which can explain the observed creation of triplet excitons from optically excited singlet states.[25]

V. CONCLUSION

The electronic properties and linear optical spectra of solid pentacene have been determined from first-principle calculations. We obtained slightly different electronic energy gaps for the two crystalline structures studied. This is attributed to enhanced intermolecular interactions in the vapor-phase structure (V) compared to the solution-phase structure (S). In addition, the binding energies of both the spin singlet and spin triplet exciton states are comparable in both the structures. The optical spectrum for structure V is in good agreement with measurements performed on pentacene thin films.

ACKNOWLEDGMENTS

This work was supported by National Science Foundation Grant No. DMR00-87088 and by the Director, Office of Science, Office of Basic Energy Sciences, Division of Materials Sciences and Engineering, U.S. Department of Energy under Contract No. DE-AC03-76SF00098. Computational resources have been provided by NSF at the National Partnership for Advanced Computational Infrastructure, and DOE at the National Energy Research Scientific Computing Center. This work is facilitated by the Computational Materials Sciences Network (CMSN) of the Department of Energy.

[1] T. Siegrist, C. Kloc, J.H. Schön, B. Batlogg, R.C. Haddon, S. Berk, and G.A. Thomas, Angew. Chem. Int. Ed. Engl. **40**, 1732 (2001).

[2] C.D. Dimitrakopoulos, A.R. Brown, and A. Pomp, J. Appl. Phys. **80**, 2501 (1996).

[3] C.C. Mattheus, A.B. Dros, J. Baas, A. Meetsma, J.L. de Boer, and T.T.M. Palstra, Acta Crystallogr., Sect. C: Cryst. Struct. Commun. **57**, 939 (2001).

[4] D. Holmes, S. Kumaraswamy, A.J. Matzger, and K.P.C. Vollhardt, Chem.-Eur. J. **5**, 3399 (1999).

[5] E. Venuti, R.G. Della Valle, A. Brillante, M. Masino, and A. Girlando, J. Am. Chem. Soc. **124**, 2129 (2002).

[6] M. Pope and C.E. Swenberg, *Electronic Processes in Organic Crystals and Polymers*, 2nd ed. (Oxford University Press, Oxford, 1999).

[7] V.M. Kenkre and P.E. Parris, Phys. Rev. B **65**, 205104 (2002); **65**, 245106 (2002).

[8] S.F. Nelson, Y.-Y. Lin, D.J. Gundlach, and T.N. Jackson, Appl. Phys. Lett. **72**, 1854 (1998).

[9] R.A. Street, D. Knipp, and A.R. Völkel, Appl. Phys. Lett. **80**, 1658 (2002).

[10] W. Warta and N. Karl, Phys. Rev. B **32**, 1172 (1985).

[11] R.B. Campbell, J.M. Robertson, and J. Trotter, Acta Crystallogr. **15**, 289 (1962).

[12] J. Ihm, A. Zunger, and M.L. Cohen, J. Phys. C **12**, 4409 (1979); see also a review article by W.E. Pickett, Comput. Phys. Rep. **9**, 115 (1989).

[13] M.S. Hybertsen and S.G. Louie, Phys. Rev. B **34**, 5390 (1986).

[14] M. Rohlfing and S.G. Louie, Phys. Rev. B **62**, 4927 (2000), and references therein.

[15] J.P. Perdew, K. Burke, and M. Ernzerhof, Phys. Rev. Lett. **77**, 3865 (1996).

[16] N. Troullier and J.L. Martins, Phys. Rev. B **43**, 1993 (1990).

[17] S. Ismail-Beigi, E.K. Chang, and S.G. Louie, Phys. Rev. Lett. **87**, 087402 (2001).

[18] J.E. Northrup, M.L. Tiago, and S.G. Louie, Phys. Rev. B **66**, 121404 (2002).

[19] J. Cornil, P.Ph. Calbert, and J.L. Brédas, J. Am. Chem. Soc. **123**, 1250 (2001).

[20] E.A. Silinsh, V.A. Kolesnikov, I.J. Muzikante, and D.R. Balode, Phys. Status Solidi B **113**, 379 (1982).

[21] E.A. Silinsh and V. Cápek, *Organic Molecular Crystals* (AIP Press, New York, 1994).

[22] S.P. Park, S.S. Kim, J.H. Kim, C.N. Whang, and S. Im, Appl. Phys. Lett. **80**, 2872 (2002).

[23] T. Aoki-Matsumoto, K. Furuta, T. Yamada, H. Moriya, K. Mizuno, and A.H. Matsui, Int. J. Mod. Phys. B **15**, 3753 (2001).

[24] Here, the Davydov splitting is understood to be the difference in excitation energy between the two lowest exciton states, which arise from the transitions involving different energy bands. For both the structures studied, we observe that the two lowest energy spin triplet excitons happen to have different band composition.

[25] C. Jundt, G. Klein, B. Sipp, J. Le Moigne, M. Joucla, and A.A. Villaeys, Chem. Phys. Lett. **241**, 84 (1995).